frontiers in Materials

ORIGINAL RESEARCH
published: 21 December 2021
doi: 10.3389/fmats.2021.790911

Glucose-Derived Carbon Nanospheres as Flame Retardant for Polyethylene Terephthalate

Jiaqian Li[1,2], Yaru Yang[1,2], Yunchao Xiao[1,2,3], Bolin Tang[1,2], Yaming Ji[1,2] and Shuqiang Liu[4]*

[1]College of Materials and Textile Engineering, Jiaxing University, Jiaxing, China, [2]Key Laboratory of Yarn Materials Forming and Composite Processing Technology of Zhejiang Province, Jiaxing University, Jiaxing, China, [3]Nanotechnology Research Institute, Jiaxing University, Jiaxing, China, [4]College of Textile Engineering, Taiyuan University of Technology, Yuci, China

To improve the flame retardant properties of polyethylene terephthalate (PET), glucose-derived carbon nanospheres (CNSs) were synthesized and introduced into PET matrix. The thermal property and flame retardancy of CNSs/PET composites were thoroughly investigated. Results showed that CNSs displayed good flame-retardant performance for PET. When blended with only 1.0 wt.% of CNSs, CNSs/PET exhibited a limiting oxygen index (LOI) of 26.3 and a vertical combustion class of V-2, and its peak-heat release rate (pk-HRR) was reduced by 41.6%. Importantly, the initial decomposition temperature and the maximum weight loss temperature of CNSs/PET were 52°C and 199°C higher than those of PET, respectively. Furthermore, a condensed phase flame-retardant mechanism appeared in CNSs/PET, which formed a dense and thermally stable protective char layer during combustion. Overall, this study disclosed the flame-retardant potential and possible mechanism of CNSs for polyesters, which would benefit the development of carbon-based materials and flame-retardant polymers.

Keywords: carbon nanospheres, polyethylene terephthalate, composite, thermal properties, flame retardant

OPEN ACCESS

Edited by:
Pingan Song,
University of Southern Queensland, Australia

Reviewed by:
Yan Zhang,
Zhejiang University, China
Bihe Yuan,
Wuhan University of Technology, China

***Correspondence:**
Yaru Yang
yyr0515@zjxu.edu.cn

Specialty section:
This article was submitted to Polymeric and Composite Materials, a section of the journal Frontiers in Materials

Received: *09 October 2021*
Accepted: *17 November 2021*
Published: *21 December 2021*

Citation:
Li J, Yang Y, Xiao Y, Tang B, Ji Y and Liu S (2021) Glucose-Derived Carbon Nanospheres as Flame Retardant for Polyethylene Terephthalate. Front. Mater. 8:790911. doi: 10.3389/fmats.2021.790911

INTRODUCTION

Polyethylene terephthalate (PET) is one of the most widely used polymer materials, involving textile, packaging and engineering plastics field (Dong et al., 2016; Zhang et al., 2020), but its flammability has brought great fire hazards to human life and property safety (Quartinello et al., 2019). Therefore, the flame retardant modification of PET is of great significance. Traditionally, halogenated compounds and phosphorus flame retardants have been widely used to endow PET with flame resistance (Quartinello et al., 2019; Zhang et al., 2021). However, most of these traditional flame retardants have defects such as toxicity, harm to the environment, and low flame retardant efficiency. For instance, as an important variety of flame retardants for polyester, halogen-based flame retardants, such as decabromodiphenyl ether (DBDPO), hexabromobenzene, have been gradually banned because of their corrosive and toxic burning products like hydrogen halide and polybrominated dibenzofurans (Xin et al., 2020). Therefore, there is an urgent need to develop new flame retardants with the characteristics of "halogen-free, eco-friendly, and low dosage" (Appavoo et al., 2020; Markwart et al., 2020; Seraji et al., 2022).

As a new type of material with abundant sources and attractive element, carbon materials have brought the revolutionary development of materials science and technology (Chen et al., 2020; Shi et al., 2021). In recent years, carbon materials have been employed as flame retardant additives for polymers (Dittrich et al., 2013a; Dittrich et al., 2013b; Wang et al., 2017; Huang et al., 2021; Yang

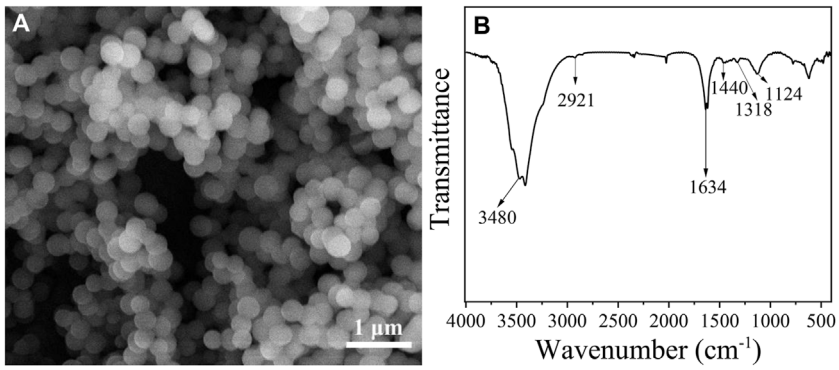

FIGURE 1 | SEM image **(A)** and FTIR spectrum **(B)** of glucose-derived CNSs.

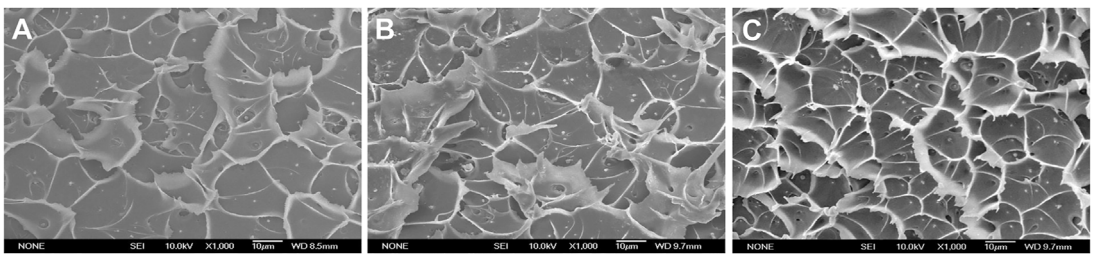

FIGURE 2 | SEM images of CNSs/PET [**(A)**-$S_{0.5}$, **(B)**-$S_{1.0}$, **(C)**-$S_{2.0}$].

et al., 2021). Among them, carbon-based nanoparticles, especially carbon nanotubes (Dittrich et al., 2013a; Wu et al., 2013; Kashiwagi et al., 2015; Shi et al., 2021), graphenes (Li et al., 2014; Yu et al., 2015; Huang et al., 2021), fullerenes (Song et al., 2009; Yang et al., 2021), etc., have attracted extensive attention due to their outstanding performance, which opened up a new way for the preparation of multifunctional flame-retardant polymer materials. Compared with traditional flame retardants, carbon-based flame retardants are more environmentally friendly and less doped. Besides, the introduction of carbon-based flame retardants can also improve the mechanical properties, thermal stability, thermal conductivity and electrical conductivity of polymers (Wang et al., 2017; Chen et al., 2018; Huang et al., 2021; Szeluga et al., 2021), which exhibit broad prospects for the development of functional polymer-based composites (He et al., 2020; Lei et al., 2022).

Carbon nanospheres (CNSs), are spherical cage-like carbon material with a fullerene structure, which can be regarded as onion-like fullerenes with a low degree of graphitization (Wang et al., 2019). The unique structure of CNSs gives them excellent properties such as small particle size, low density, excellent electrical conductivity, thermal conductivity, thermal stability and chemical stability (Yang et al., 2021). What's more, CNSs are environmentally-friendly, simple in preparation, low in production cost, and suitable for industrial production with raw materials ranging from glucose, starch to wood (Tsubota et al., 2014; Seo et al., 2016). So far, CNSs have been mainly used in lithium ion battery electrode materials, photovoltaic materials, catalyst carriers, and super capacitors (Kwon et al., 2019; Xiong et al., 2020), but the application of CNSs in flame retardant remains to be further explored and flame-retardant mechanism of CNSs is still unclear in PET matrix.

In the present study, glucose-derived CNSs were firstly synthesized and characterized. And the synthesized CNSs were introduced into PET matrix by melt blending to prepare CNSs/PET composite. The flame retardancy, char formation behavior, thermal degradation performance and flame retardance of CNSs/PET have been studied in detail to reveal the flame-retardant potential and possible flame-retardant mechanism of CNSs.

EXPERIMENTAL

Materials

Glucose (Analytical Reagent) was provided by Tianjin Hengxing Chemical Reagent co., LTD. (China). Distilled water was self-made in laboratory. PET chips (SD 500) with a viscosity index (VI) of 0.68 dl/g were purchased from Sinopec Yizheng co., LTD. (China). All the materials were used as received without any further purification.

Synthesis of Glucose-Derived CNSs

For the synthesis of carbon spheres, chemical vapor deposition method, solvothermal (or hydrothermal) method and template

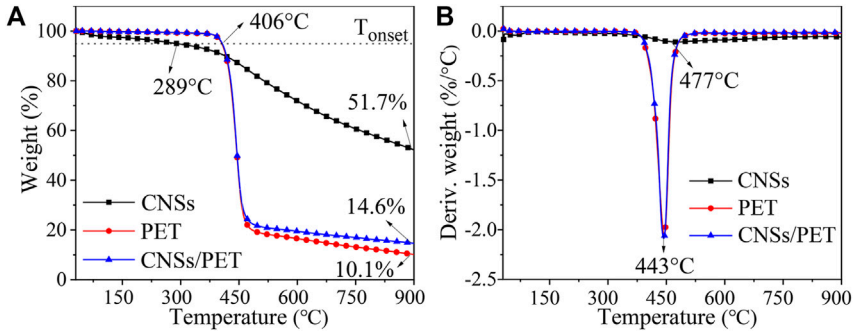

FIGURE 3 | TG **(A)** and DTG **(B)** curves of CNSs, PET and CNSs/PET.

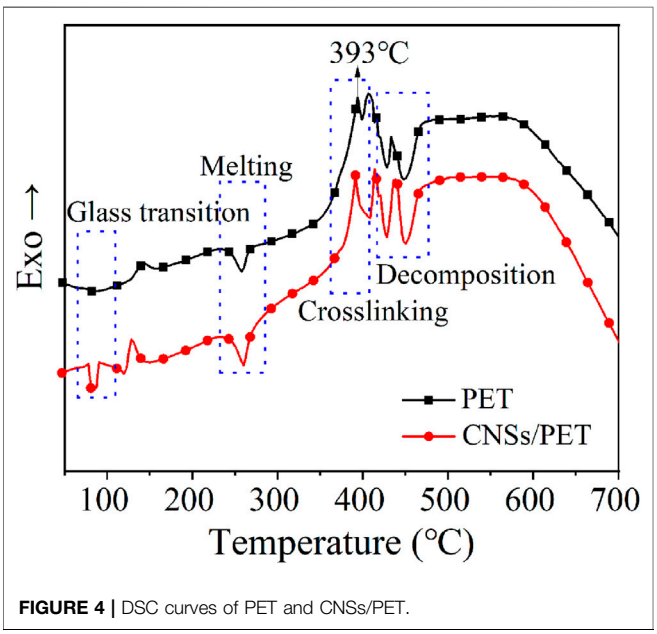

FIGURE 4 | DSC curves of PET and CNSs/PET.

method, are the most commonly-used methods. Among them, the hydrothermal method produces carbon spheres with advantages of uniform morphology, good dispersibility, high yield and low cost (Mi et al., 2008). After a series of attempts and comparison, a glucose hydrothermal method was finally selected to prepare CNSs. Briefly, glucose solution (0.4 mol/L) was transferred into high-pressure reactor for hydrothermal reaction. After stirring (150 r/min) for 4 h under 280°C, the heating system is turned off, cooled down to room temperature under constant stirring; the reactant was taken out from the reactor, followed by filtration and washing with distilled water; the final products of CNSs were harvested after vacuum drying at 120°C for 4 h and grinding.

Preparation of CNSs/PET Composites

The CNSs/PET composites were prepared by melt blending in a twin-screw extruder (CET35-40D). PET and CNSs were dried at 120°C for 12 h before use. The section temperature of twin-screw extruder was set as 270°C, 272, 273, 275, 280, 287, 280, 282 and 284°C, and the feed rate was 15 rpm. The limiting oxygen index (LOI) and vertical burning test specimens were prepared using an injection molding machine (JH600), the temperature of each section for injection molding was 255, 254, 253, and 251°C. The cone calorimeter test specimens were prepared using a flat-panel curing machine (VT-LH20A). CNSs/PET composites containing 0.5 wt.%, 1.0% wt.% and 2.0 wt.% CNSs were designated as S0.5, S1.0, and S2.0, respectively.

Characterization

The morphology of synthesized CNSs was observed using JSM-6510LA field emission scanning electron microscope (SEM) with the accelerating voltage of 10 kV, and the CNSs were sputtered with gold for 35 s before observation. The Perkin-Elmer Frontier fourier transform infrared spectrometer (FTIR) was used to determine the surface properties and chemical structure of CMSs with a scan range of 4,000~400 cm^{-1}.

LOI were measured at room temperature using a TM606 oxygen index meter according to ISO 4589-2:2006 standard with specimen dimension of 130 × 6.5 × 3 mm^3. Vertical burning tests were conducted on a CZF-5-type burning instrument according to ICE 60695-11-10 test standard with specimen dimension of 130 × 13 × 3 mm^3.Cone calorimeter measurements were performed on an FTT cone calorimeter according to ISO 5660-1 under an external heat flux of 50 kW/m^2. The dimension of samples was 100 × 100 × 3 mm^3. The micromorphology images of burned PET and CNSs/PET were obtained using SEM. The thermal stability of residues from the cone calorimeter test was determined *via* a Perkin-Elmer TG 4000 thermogravimetric analyzer at the heating rate of 10°C/min under the nitrogen atmosphere from 30 to 900°C.Thermogravimetric analyses (TG) were performed using Perkin-Elmer TG 4000 thermogravimetric analyzer at the heating rate of 10, 20, 30, 40°C/min, respectively under the nitrogen atmosphere from 30 to 900°C. The mass of each sample was 5 ± 0.5 mg. Combination characterization of thermogravimetry and differential scanning calorimeter (TG-DSC) tests were performed using Netzsch STA449 type DSC-TG combined instrument at the heating rate of 10°C/min under argon atmosphere from 30 to 900°C. The mass of each sample was 10 ± 0.5 mg. Pyrolysis gas chromatography-mass spectrometry (Py-GC/MS) tests were performed using gas chromatography (Agilent 6980N) and

mass spectrometer (Agilent 5975). The pyrolysis chamber was under helium atmosphere, the relevant samples (300 mg) were heated from ambient temperature to 750°C at a rate of 200°C/min and kept for 20 s. The carrier gas was helium. For the operation, the temperature program of the capillary column (HP-5MS) of GC was as follows: 5 min at 50°C, the temperature increased to 260°C at a rate of 10°C/min then kept at 260°C for 10 min. The injector temperature was 220°C. Mass spectra (MS) indicator was operated in the electron impact mode at the electron energy of 70 eV. The detection of MS was carried out using NIST library.

RESULTS AND DISCUSSION

Synthesis and Characterization of Glucose-Derived CNSs

In this study, glucose-derived CNSs were firstly synthesized *via* a hydrothermal method, and the morphology and structure of CNSs were characterized. As can be seen in **Figure 1A**, the synthesized CMSs are spherical particles with smooth surface, uniform size distribution, and an average diameter of 310.2 nm. FTIR spectrum of CMSs is shown in **Figure 1B**. Peak at 3480 cm^{-1} corresponds to the O-H stretching vibration peak; Peaks at 2921 and 1440 cm^{-1} correspond to the O-H stretching vibration and bending vibration peaks of carboxyl, respectively; Peak at 1634 cm^{-1} is attributed to the stretching vibration peak of -C=O-; Peak at 1318 cm^{-1} corresponds to the stretching vibration peak of C-O in carboxyl. All these characteristic peaks indicate that glucose-derived CNSs have sufficient hydroxyl and carboxyl groups on the surface, which benefit further surface modification of CNSs.

Dispersion of CNSs in PET Matrix

To investigate the flame-retardant property of glucose-derived CNSs, the synthesized CNSs were introduced into PET matrix by melt blending. In the first place, tensile cross-sectional morphologies of CNSs/PET composites were observed by SEM. As shown in **Figure 2A–C**, the tensile cross-section of CNSs/PET display a typical ductile fracture morphology, indicating good compatibility between CNSs and PET matrix. In addition, there is no apparent CNS aggregation appearing on cross-section surface, suggesting the acceptable dispersion of CNSs in PET matrix.

Thermal Degradation Behavior of PET and CNSs/PET

TG Analysis

The combustion behavior of polymers is closely related to their thermal degradation behavior, and the carbon slag produced by polymer degradation directly affects the transfer of heat flow and mass flow, so the carbonization of the polymer is an important factor affecting its flame retardancy (Chen et al., 2013). Thus, TG analysis was performed on PET and CNSs/PET.

Figure 3 shows the TG and DTG curves of CNSs, PET and CNSs/PET ($S_{1.0}$) under nitrogen atmosphere. As demonstrated in TG curves, the main weight loss stages of CNSs/PET and PET almost overlap, and the T_{onset} and T_{max} of the both are basically the same. But it should be noted that the $C_{R900°C}$ of PET is 10.1%, while the $C_{R900°C}$ of CNSs/PET is increased to 14.6%, which suggests that CNSs promote the carbonization of PET.

In order to further clarify the role of CNSs in promoting the carbonization of PET, the theoretical value of the residual char content was calculated ($C_{R900°C, cal}$) (Chen et al., 2013). Results showed that the actual residual-char content (14.6%) of CNSs/PET was 39.0% higher than the theoretical value ($C_{R900°C, cal}$ = 10.5%), which demonstrates that CNSs could act as char-forming agent for PET.

TG-DSC Analysis

Cross-linking of polymers directly affects their rheology, melting droplets, and self-extinguishing behavior (Dong et al., 2016). In order to study the effect of CNSs on the cross-linking behavior of PET during thermal degradation, TG-DSC combined analysis was conducted on PET and CNSs/PET ($S_{1.0}$). The obtained DSC curves of the two during thermal degradation are shown in **Figure 4**.

As showed in **Figure 4**, there is an upward exothermic peak near 393°C in the DSC curves of both PET and CNSs/PET, which is a cross-linked peak of PET (Du et al., 2017). It is worth noting that the crosslinking peak of CNSs/PET is significantly larger than that of PET, and the crosslinking temperature range of CNSs/PET is wider, which indicates that CNSs promoted the crosslinking of PET. As we all know, PET is a type of straight-chain macromolecule, which is difficult to chemically crosslink itself. This means in the early stage of PET degradation, the presence of CNSs serves as a physical cross-linking point, thereby forming a cross-network *in situ* in PET, and this phenomenon will be confirmed by subsequent investigation. Additionally, the crosslinking temperature is near to the initial degradation temperature of PET, suggesting that the crosslinking occurred at the initial stage of thermal degradation.

Py-GC-MS Analysis

In order to examine the impact of CNSs on the thermal pyrolysis of PET, Py-GC-MS analysis was performed on PET and CNSs/PET ($S_{1.0}$). (See supporting information for the Py-GC spectra and main pyrolysis products at 750°C of PET and CNSs/PET).

Table 1 shows the comparison of pyrolysis products at 750°C of PET and CNSs/PET. It is shown that the pyrolysis products present in both PET and CNSs/PET are mainly substances containing -C=C-, ester groups or carboxyl groups. From the formation of these products, it can be seen that the primary pyrolysis mechanism of CNSs/PET and PET is consistent, starting from the six-membered cyclic transition state randomly breaking into two primary pyrolysis products of long-chain acetyl acid and vinyl ester (Buxbaum, 1968). And the decomposition mechanism diagram of PET is deduced and provided in the Supplementary Material (**Supplementary Figure S2**). Compared with neat PET, the unique pyrolysis products generated from CNSs/PET are mainly oxygen-containing structural units, branched structural units, conjugated aromatic

TABLE 1 | Comparison of pyrolysis products at 750°C of PET and CNSs/PET.

Common pyrolysis products of PET and CNSs/PET	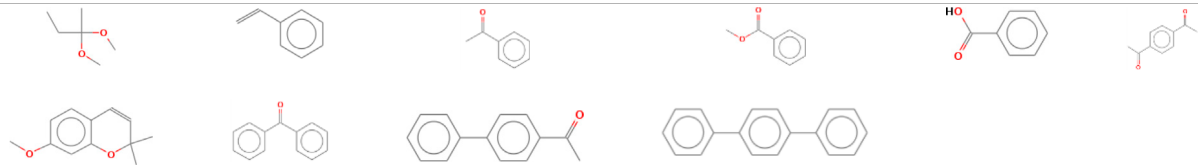
Exclusive pyrolysis products of CNSs/PET	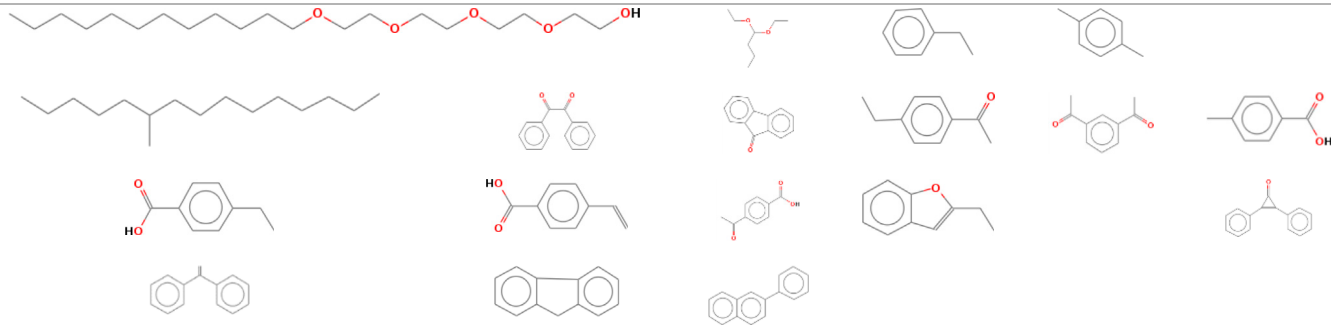

TABLE 2 | LOI and vertical burning test results of CNSs/PET.

Samples	LOI (%)	t_1[a]	t_2[b]	t_f[c]	Cotton ignition	Rate
PET	21.0	>150	>100	—	Yes	NR
CNSs/PET ($S_{0.5}$)	24.1	2.6	2.5	25.5	Yes	V-2
CNSs/PET ($S_{1.0}$)	26.3	2.4	2.4	24.0	Yes	V-2
CNSs/PET ($S_{2.0}$)	23.4	2.4	2.8	26.0	Yes	V-2

[a]*Average combustion times after the first application of the flame.*
[b]*Average combustion times after the second application of the flame.*
[c]*The total duration (five specimens) of flaming.*

rings, heterocyclic or fused ring structural units, and some structural units with vinyl groups. The increase of oxygen-containing structural units proves that the presence of CNSs inhibited the degradation of PET. The increase in branching and cyclization products is mainly related to the micro-blocking effect of CNSs and the cross-network formed in PET. Related studies (Spanninger, 1974; Giraud et al., 2012) showed that the main components of the non-combustible coke resulting from the combustion of PET are conjugated aromatic ring, heterocyclic ring and condensed ring structural units. Coincidentally, there are more such products in the pyrolysis products of CNSs/PET, which provide a sufficient material basis for the generation of the char layer with flame retardant effect. This result corroborates the role of CNSs in promoting the char formation of PET.

LOI and Vertical Burning Test Analysis

The LOI and vertical burning test results are presented in **Table 2**. As shown in **Table 2**, the LOI of PET is only 21.0%, and the LOI values of CNSs/PET composites increase first and then decrease with the increase of CNSs dosage, which reaches a maximum of 26.3 with 1.0 wt.% CNSs. This is very similar to the performance of graphene oxide (GO) in flame retardant polymer, that a small amount of GO can effectively improve the flame retardancy of polymers (Dittrich et al., 2013b; Hu and Zhang, 2014; Li et al., 2014; Hu et al., 2015), however, increasing the amount of GO is not conducive to the flame retardancy of the polymer. Kim et al. (2010), Shi and Li (2011) and this phenomenon is probably due to the heat concentration caused by CNSs agglomeration, which reduces the flame retardant properties of the CNSs/PET with a high CNSs dosage. **Table 2** also shows the vertical burning test results. It can be seen that the introduction of CNSs significantly shortens the afterburning time of PET, which is related to the increase in heat capacity and the change in melt viscosity. Although all t_1, t_2 and t_f of CNSs/PET has been greatly shortened, it is a pity that the melt drop of CNSs/PET ignited the cotton. Thus, CNSs/PET can only reach V-2 level.

Cone Calorimeter Test Analysis

Further, cone calorimeter test was conducted to determine heat release rate (HRR) and total heat release (THR) of PET and CNSs/PET. As shown in **Figure 5** and **Table 3**, the HRR and THR curves of CNSs/PETs are significantly lower than that of PET (**Figure 5**). The peak of HRR (pk-HRR) of PET is 559.9 kW/m^2, while the pk-HRR of CNSs/PET decreases to 327.3 kW/m^2 with a reduction of 41.6% at only 1.0 wt.% CNSs dosage. Furthermore, the time to pk-HRR of CNSs/PETs was also significantly prolonged, and the potential fire hazard parameter TTI/pk-HRR is increased from 0.07 m^2 s/kW of neat PET to 0.18 m^2 s/kW of CNSs/PET (**Table 3**), suggesting that CNSs could generate an obvious flame inhibition effect during combustion.

Moreover, we can acquire the development of the char layer in the combustion process from the shape of the HRR curves. The HRR curve of PET has a sharp peak shape which drops dramatically after reaching the pk-HRR, indicating that there is no effective char layer protection during the combustion. While the HRR curve of CNSs/PET has a bald shape, and there is a plateau in the HRR curve of $S_{1.0}$, indicating that a protective layer is likely to be formed during the combustion process. Furthermore, the THR reduction of CNSs/PET also implies that CNSs can promote the char formation of PET.

The residue after combustion is another important indicator to analyze the flame-retardant mechanism. As listed in **Table 3**, the residue of PET is only 11.5%, while the residue of the three CNSs/PET composites is sequentially increased to 12.2, 20.0, and 18.3%. This proves that CNSs have a condensed phase flame retardant effect on PET. In addition, **Table 3** also provides av-CO and CO_2 results. In comparison with PET, CNSs/PET have larger yield (av-CO) and less CO_2 yield (av-CO_2), demonstrating that the combustion degree of CNSs/PET is lower than that of PET, and gas phase flame-retardant activities are more likely occurred during combustion (Bao et al., 2012; Schartel et al., 2016). As for the time to ignition (TTI), **Table 3** shows that the TTI of $S_{0.1}$ is longer than 46% by comparison with PET, which represents an

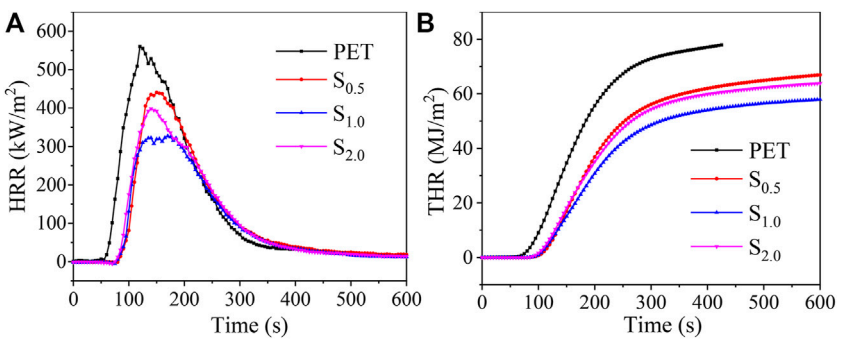

FIGURE 5 | The HRR **(A)** and THR **(B)** curves of PET and CNSs/PET.

TABLE 3 | Cone calorimeter test data of PET and CNSs/PET (50 kW/m^2).

Samples	PET	$S_{0.5}$	$S_{1.0}$	$S_{2.0}$
TTI (s)	41	55	60	52
pk-HRR (kW/m^2)	559.9	440.5	327.3	398.3
Time to pk-HRR (s)	120	150	170	140
THR (MJ/m^2)	77.8	67.1	59.9	63.9
Residue (wt.%)	11.5	12.2	20.0	18.3
av-CO yield	0.05	0.06	0.07	0.06
av-CO_2 yield	1.26	1.20	0.99	1.16
TTI/pk-HRR	0.07	0.12	0.18	0.13

increase in flame resistance. Similar to the results of LOI, the TTI of CNSs/PET tends to decrease as the CNSs dosage increases from 1.0wt.% to 2.0%, and this phenomenon may be caused by the violent thermal reaction due to the agglomeration of CNSs in PET matrix.

Flame Retardant Mechanism

Based on the above analysis, morphology and thermal stability of the char layer were further investigated to reveal the flame retardant mechanism. **Figure 6** represents a visual comparison of PET and CNSs/PET ($S_{1.0}$) after vertical combustion test. As shown in **Figure 6**, the lower half of PET shows a wire-like shape after burning, while CNSs/PET has a water-drop shape. Related research (Bao et al., 2012) attributed this phenomenon to that carbon materials can form a network structure on the surface of the polymer during combustion, thereby restraining the flow of the melt. In addition, the upper half of PET also undergoes severe melt deformation. In contrast, there are more black char layers covering the surface of CNSs/PET, so that its upper half is well protected. This visually demonstrates that promoting the formation of effective char layer is an important approach to achieve flame retardant.

Further, from the partial enlarged view of the samples (**Figure 6**), it can be seen that the surface of the original CNSs/PET samples is smooth, but a large number of solid carbon particles are embedded on the surface after burning. This can be attributed to the fact that during the combustion of CNSs/PET, the high surface energy enables CNSs to migrate onto the surface of the melt as PET matrix is ablated, and thus promote the formation of carbon residue particles on the PET surface.

Figure 7 compares the digital photos and SEM images of PET and CNSs/PET after the cone calorimeter test. It can be seen that the char layer of PET (**Figures 7A,A1**) is loose and porous. In contrast, the density of the CNSs/PET char layer has been significantly improved. In addition, **Figure 7B** shows that a puffy coking charred layer is formed by CNSs/PET, and the puffy coking charred layer has lots of closed bubbles, which can effectively suppress the diffusion of gas and further play a role in heat insulation (Zhang et al., 2010), thus preventing heat and mass transfer during combustion. It is worth noting that many solid carbon particles are embedded in the char layer of CNSs/PET (**Figure 7B1**), and these particles are not observed in the char layer of PET. This further verifies that CNSs can promote the generation of carbon slag particles on the PET surface, similar to the flame retardant mechanism of clay (Kiliaris and Papaspyrides, 2010).

Figure 8 shows the TG-DTG curves of the char residue of PET and CNSs/PET. There are three apparent weight loss stages of the char residue of PET. The first stage occurs before 357°C,

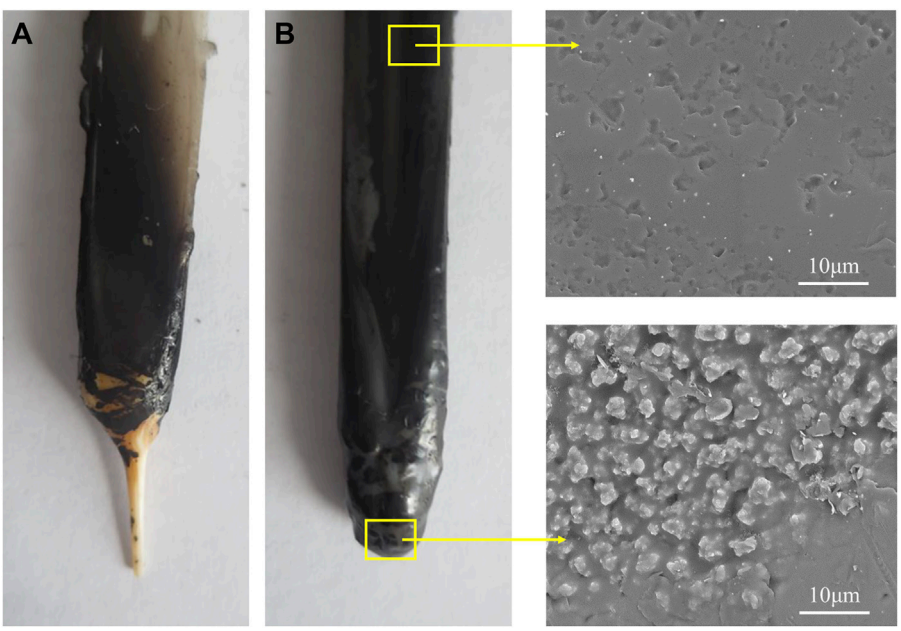

FIGURE 6 | The morphology of PET **(A)** and CNSs/PET **(B)** after vertical combustion test.

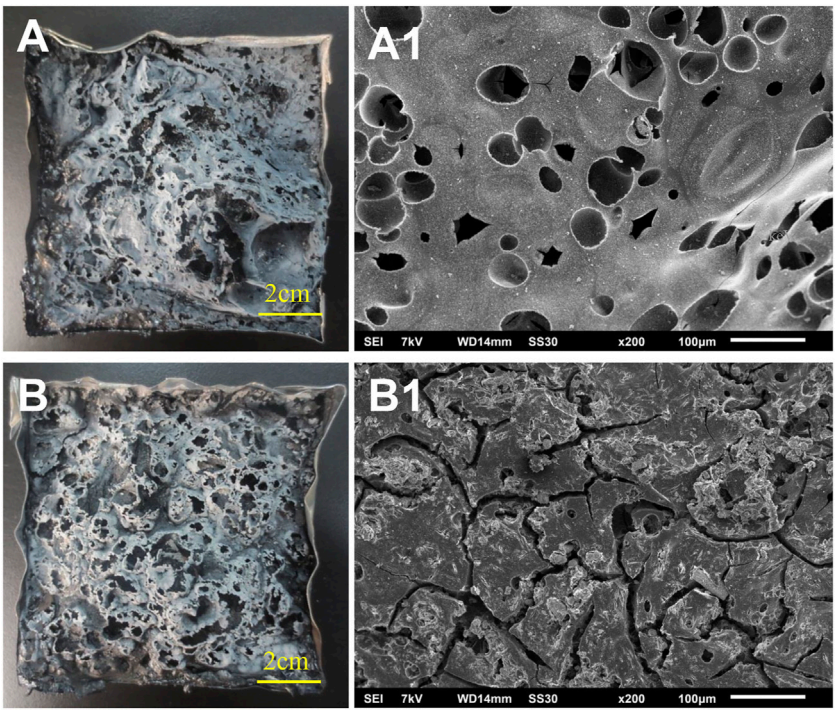

FIGURE 7 | Digital photo [**(A)**-PET, **(B)**-CNSs/PET] and SEM images [**(A1)**-PET, **(B1)**-CNSs/PET] of char residues after cone calorimeter test.

corresponding to the degradation of highly degradable small molecule combustion products present in its char residue. The second stage arises between 357 and 513°C, corresponding to the incomplete carbides further degraded into coke-like products with higher thermal stability. The third stage appears after 513°C, which corresponds to the further degradation of coke-like substances. However, the TG curve of the char residue of CNSs/PET is gentle before 513°C. Additionally, we note that there is almost no weight loss except for a slight weight loss caused by the decomposition of the small molecule combustion products present in the char residue. This certifies that the char residue of CNSs/PET could bear higher flame temperature when burning. Besides, the DTG curve of the char residue of CNSs/PET does not show a second weight loss peak between 357 and 513°C compared with that of PET, indicating that the char residue structure of CNSs/PET is much more stable. The initial decomposition temperature (T_{onset}, denoted as the temperature at which the weight loss is 5%) and the maximum weight loss

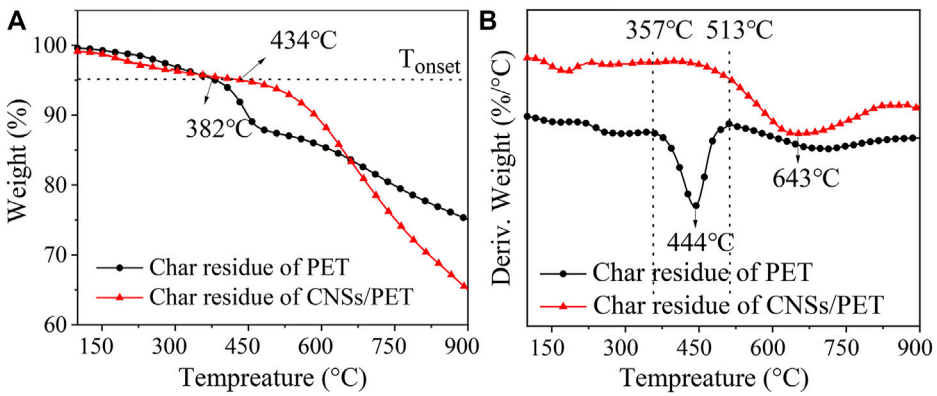

FIGURE 8 | TG **(A)** and DTG **(B)** curves of char residue of PET and CNSs/PET.

temperature (T_{max}) of the char residue of CNSs/PET are 434°C and 643°C, respectively, are 52°C and 199°C higher than those of PET. This fully proves that the thermal stability of the char residue formed by the combustion of PET is significantly improved by the introduction of CNSs.

Taking all these results together, flame retardant mechanism of CNSs/PET can be revealed. When CNSs/PET is heated to melt, the large surface energy of CNSs promotes themselves migrate to the surface of PET. Meanwhile, CNSs act as physical crosslink points in PET and promote the formation of crosslinked structures. At the same time, the difficult-flammable solid carbonaceous particles formed by the degradation of CNSs are embedded in the char layer to stabilize the structure of the char layer. The char layer covers on the polymer surface, thereby protecting the interior matrix from burning.

CONCLUSION

In conclusion, with uniform morphology and good dispersibility, glucose-derived CNSs can be simply synthesized *via* a hydrothermal method. The introduction of CNSs was able to effectively enhance the flame retardancy of PET, and CNSs exhibited considerable performance in reducing the heat release rate of PET and promoting char formation. Further, CNSs were determined to have a typical condensed-phase flame-retardant mechanism accompanied with some gas-phase flame retardation effect. On one hand, CNSs impacted the thermal decomposition and cross-linking behavior of PET to generate a dense char layer with high thermal stability. On the other hand, cone calorimeter results revealed the changes in gas production during combustion. In short, this study presents the flame-retardant potential and promising application of CNSs in flame-retardant modification of polymers.

DATA AVAILABILITY STATEMENT

The original contributions presented in the study are included in the article/**Supplementary Material**, further inquiries can be directed to the corresponding author.

AUTHOR CONTRIBUTIONS

JL conducted the synthesis and characterization. YY designed the experiment, analyzed the results, and provided founding and project administration. YX performed writing-review and editing. BT, YJ, and SL discussed the analysis of the data and contributed to the writing of the manuscript. All authors contributed to the writing of the manuscript and have given approval to the submitted manuscript.

FUNDING

This work was financially supported by Natural Science Foundation of Zhejiang Province (Grant No. LQ21E030008 and LQ22C100002); National College Student Innovation and Entrepreneurship Training Program of Jiaxing University (Grant No. CD851920510); Student Research and Training (SRT) Project of Jiaxing University (CD8517203298); Open Project Program of Key Laboratory of Yarn Materials Forming and Composite Processing Technology of Zhejiang Province (Grant No. MTC 2020-09).

SUPPLEMENTARY MATERIAL

The Supplementary Material for this article can be found online at: https://www.frontiersin.org/articles/10.3389/fmats.2021.790911/full#supplementary-material

REFERENCES

Appavoo, D., Amarnath, N., and Lochab, B. (2020). Cardanol and Eugenol Sourced Sustainable Non-halogen Flame Retardants for Enhanced Stability of Renewable Polybenzoxazines. *Front. Chem.* 8, 711. doi:10.3389/fchem.2020.00711

Bao, C., Guo, Y., Yuan, B., Hu, Y., and Song, L. (2012). Functionalized Graphene Oxide for Fire Safety Applications of Polymers: a Combination of Condensed Phase Flame Retardant Strategies. *J. Mater. Chem.* 22, 23057–23063. doi:10.1039/c2jm35001g

Buxbaum, L. H. (1986). The Degradation of Poly(ethylene Terephthalate). *Angew. Chem. Int. Edition* 7, 182–190. doi:10.1002/anie.19680182

Chen, C., Zhao, X., Shi, C., and Chen, J. (2018). Synergistic Effect between Carbon Nanoparticle and Intumescent Flame Retardant on Flammability and Smoke Suppression of Copolymer Thermoplastic Polyurethane. *J. Mater. Sci.* 53, 6053–6064. doi:10.1007/s10853-017-1970-0

Chen, S., Li, J., Zhu, Y., Guo, Z., and Su, S. (2013). Increasing the Efficiency of Intumescent Flame Retardant Polypropylene Catalyzed by Polyoxometalate Based Ionic Liquid. *J. Mater. Chem. A.* 1, 15242–15246. doi:10.1039/c3ta13538a

Chen, S., Yang, G., Zhao, X., Wang, N., Luo, T., Chen, X., et al. (2020). Hollow Mesoporous Carbon Spheres for High Performance Symmetrical and Aqueous Zinc-Ion Hybrid Supercapacitor. *Front. Chem.* 8, 663. doi:10.3389/fchem.2020.00663

Dittrich, B., Wartig, K.-A., Hofmann, D., Mülhaupt, R., and Schartel, B. (2013a). Carbon Black, Multiwall Carbon Nanotubes, Expanded Graphite and Functionalized Graphene Flame Retarded Polypropylene Nanocomposites. *Polym. Adv. Technol.* 24, 916–926. doi:10.1002/pat.3165

Dittrich, B., Wartig, K.-A., Hofmann, D., Mülhaupt, R., and Schartel, B. (2013b). Flame Retardancy through Carbon Nanomaterials: Carbon Black, Multiwall Nanotubes, Expanded Graphite, Multi-Layer Graphene and Graphene in Polypropylene. *Polym. Degrad. Stab.* 98, 1495–1505. doi:10.1016/j.polymdegradstab.2013.04.009

Dong, X., Chen, L., Duan, R.-T., and Wang, Y.-Z. (2016). Phenylmaleimide-containing PET-Based Copolyester: Cross-Linking from 2π + π Cycloaddition toward Flame Retardance and Anti-dripping. *Polym. Chem.* 7, 2698–2708. doi:10.1039/c6py00183a

Du, Y., Jiang, X., Lv, G., Jin, Y., Wang, F., Chi, Y., et al. (2017). TG-DSC and FTIR Study on Pyrolysis of Irradiation Cross-Linked Polyethylene. *J. Mater. Cycles Waste Manag.* 19, 1400–1404. doi:10.1007/s10163-016-0530-z

Giraud, S., Devaux, E., and Capon, G. (2012). Thermal and Fire Resistance of Fibrous Materials Made by PET Containing Flame Retardant Agents. *Polym. Degrad. Stab.* 97, 2545–2551.

He, W., Song, P., Yu, B., Fang, Z., and Wang, H. (2020). Flame Retardant Polymeric Nanocomposites through the Combination of Nanomaterials and

Conventional Flame Retardants. *Prog. Mater. Sci.* 114, 100687. doi:10.1016/j.pmatsci.2020.100687

Hu, J., and Zhang, F. (2014). Self-assembled Fabrication and Flame-Retardant Properties of Reduced Graphene Oxide/waterborne Polyurethane Nanocomposites. *J. Therm. Anal. Calorim.* 118, 1561–1568. doi:10.1007/s10973-014-4078-7

Hu, W., Yu, B., Jiang, S.-D., Song, L., Hu, Y., and Wang, B. (2015). Hyper-branched Polymer Grafting Graphene Oxide as an Effective Flame Retardant and Smoke Suppressant for Polystyrene. *J. Hazard. Mater.* 300, 58–66. doi:10.1016/j.jhazmat.2015.06.040

Huang, G., Chen, W., Wu, T., Guo, H., Fu, C., Xue, Y., et al. (2021). Multifunctional Graphene-Based Nano-Additives toward High-Performance Polymer Nanocomposites with Enhanced Mechanical, thermal, Flame Retardancy and Smoke Suppressive Properties. *Chem. Eng. J.* 410, 127590. doi:10.1016/j.cej.2020.127590

Kashiwagi, T., Grulke, E., Hilding, J., Harris, R., Awad, W., and Douglas, J. (2015). Thermal Degradation and Flammability Properties of Poly(propylene)/carbon Nanotube Composites. *Macromolecular Rapid Commun.* 23, 761–765. doi:10.1002/1521-3927(20020901)23:13<761::AID-MARC761>3.0.CO;2-K

Kiliaris, P., and Papaspyrides, C. D. (2010). Polymer/layered Silicate (clay) Nanocomposites: An Overview of Flame Retardancy. *Prog. Polym. Sci.* 35, 902–958. doi:10.1016/j.progpolymsci.2010.03.001

Kim, F., Luo, J., Cruz-Silva, R., Cote, L. J., Sohn, K., and Huang, J. (2010). Self-propagating Domino-like Reactions in Oxidized Graphite. *Adv. Funct. Mater.* 20, 2867–2873. doi:10.1002/adfm.201000736

Kwon, H.-N., Park, G. D., Kang, Y. C., and Roh, K. C. (2019). Fabrication of Bimodal Micro-mesoporous Amorphous Carbon-Graphitic Carbon-Reduced Graphene Oxide Composite Microspheres Prepared by Pilot-Scale spray Drying and Their Application in Supercapacitors. *Carbon* 144, 591–600. doi:10.1016/j.carbon.2018.12.111

Lei, L., Menghe, Z., Ma, Z., Xiaodong, X., Mohse, S. S., Bin, Y., et al. (2022). A Reactive Copper-Organophosphate-MXene Heterostructure Enabled Antibacterial, Fire-Retardant and Mechanically Robust Polymer Nanocomposites. *Chem. Eng. J.* 430, 132712. doi:10.1016/j.cej.2021.132712

Li, K.-Y., Kuan, C.-F., Kuan, H.-C., Chen, C.-H., Shen, M.-Y., Yang, J.-M., et al. (2014). Preparation and Properties of Novel Epoxy/graphene Oxide Nanosheets (GON) Composites Functionalized with Flame Retardant Containing Phosphorus and Silicon. *Mater. Chem. Phys.* 146, 354–362. doi:10.1016/j.matchemphys.2014.03.037

Markwart, J. C., Battig, A., Urbaniak, T., Haag, K., Koschek, K., Schartel, B., et al. (2020). Intrinsic Flame Retardant Phosphonate-Based Vitrimers as a Recyclable Alternative for Commodity Polymers in Composite Materials. *Polym. Chem.* 11, 4933–4941. doi:10.1039/d0py00275e

Mi, Y., Hu, W., Dan, Y., and Liu, Y. (2008). Synthesis of Carbon Micro-spheres by a Glucose Hydrothermal Method. *Mater. Lett.* 62, 1194–1196. doi:10.1016/j.matlet.2007.08.011

Quartinello, F., Kremser, K., Vecchiato, S., Schoen, H., Vielnascher, R., Ploszczanski, L., et al. (2019). Increased Flame Retardancy of Enzymatic Functionalized PET and Nylon Fabrics via DNA Immobilization. *Front. Chem.* 7, 685. doi:10.3389/fchem.2019.00685

Schartel, B., Perret, B., Dittrich, B., Ciesielski, M., Krämer, J., Müller, P., et al. (2016). Flame Retardancy of Polymers: The Role of Specific Reactions in the Condensed Phase. *Macromol. Mater. Eng.* 301, 9–35. doi:10.1002/mame.201500250

Seo, H. J., Kim, S., Huh, W., Park, K.-W., Lee, D. R., Son, D. W., et al. (2016). Enhancing the Flame-Retardant Performance of wood-based Materials Using Carbon-Based Materials. *J. Therm. Anal. Calorim.* 123, 1935–1942. doi:10.1007/s10973-015-4553-9

Seraji, S. M., Song, P., Varley, R. J., Bourbigot, S., Voice, D., and Wang, H. (2022). Fire-retardant Unsaturated Polyester Thermosets: The State-Of-The-Art, Challenges and Opportunities. *Chem. Eng. J.* 430, 132785. doi:10.1016/j.cej.2021.132785

Shi, C., Qian, X., Jing, J., and Che, H. (2021). Functionalized CNTs with DOPO and Silicon Containing Agents: Effective Reinforcer for thermal and Flame Retardant Properties of Polystyrene Nanocomposites. *Front. Chem.* 8, 627642. doi:10.3389/fchem.2020.627642

Shi, Y., and Li, L.-J. (2011). Chemically Modified Graphene: Flame Retardant or Fuel for Combustion? *J. Mater. Chem.* 21, 3277–3279. doi:10.1039/c0jm02953j

Song, P. a., Liu, H., Shen, Y., Du, B., Fang, Z., and Wu, Y. (2009). Fabrication of Dendrimer-like Fullerene (C60)-Decorated Oligomeric Intumescent Flame Retardant for Reducing the thermal Oxidation and Flammability of Polypropylene Nanocomposites. *J. Mater. Chem.* 19, 1305–1308. doi:10.1039/b815610g

Spanninger, P. A. (1974). Thermoxidative Degradation Leading to Gel in Poly(ethylene Terephthalate). *J. Polym. Sci. Polym. Chem. Ed.* 12, 709–717. doi:10.1002/pol.1974.170120401

Szeluga, U., Pusz, S., Kumanek, B., Olszowska, K., Kobyliukh, A., and Trzebicka, B. (2021). Effect of Graphene Filler Structure on Electrical, thermal, Mechanical, and Fire Retardant Properties of Epoxy-Graphene Nanocomposites - a Review. *Crit. Rev. Solid State. Mater. Sci.* 46, 152–187. doi:10.1080/10408436.2019.1708702

Tsubota, T., Morita, M., Murakami, N., and Ohno, T. (2014). Performance of Carbon Material Derived from Starch Mixed with Flame Retardant as Electrochemical Capacitor. *J. Power Sourc.* 267, 635–640. doi:10.1016/j.jpowsour.2014.05.140

Wang, H., Qiu, X., Wang, W., Jiang, L., and Liu, H. (2019). Iron Sulfide Nanoparticles Embedded into a Nitrogen and Sulfur Co-doped Carbon Sphere as a Highly Active Oxygen Reduction Electrocatalyst. *Front. Chem.* 7, 855. doi:10.3389/fchem.2019.00855

Wang, X., Kalali, E. N., Wan, J.-T., and Wang, D.-Y. (2017). Carbon-family Materials for Flame Retardant Polymeric Materials. *Prog. Polym. Sci.* 69, 22–46. doi:10.1016/j.progpolymsci.2017.02.001

Wu, Z., Xue, M., Wang, H., Tian, X., Ding, X., Zheng, K., et al. (2013). Electrical and Flame-Retardant Properties of Carbon Nanotube/poly(ethylene Terephthalate) Composites Containing Bisphenol A Bis(diphenyl Phosphate). *Polymer* 54, 3334–3340. doi:10.1016/j.polymer.2013.04.051

Xin, W., Zhiqi, L., Zhi, L., Jing, Z., De-Yi, W., Karolina, S., et al. (2020). Constructing Multifunctional Nanofiller with Reactive Interface in PLA/CB-g-DOPO Composites for Simultaneously Improving Flame Retardancy, Electrical Conductivity and Mechanical Properties. *Composites Sci. Technology* 188, 107988. doi:10.1016/j.compscitech.2019.107988

Xiong, W., Zhang, J., Xiao, Y., Zhu, Y., Wang, Z., and Lu, Z. (2020). Oxygen-rich Nanoflake-Interlaced Carbon Microspheres for Potassium-Ion Battery Anodes. *Chem. Commun. (Camb)* 56, 3433–3436. doi:10.1039/d0cc00357c

Yang, Y., Diaz Palencia, J. L., Wang, N., Jiang, Y., and Wang, D. Y. (2021). Nanocarbon-based Flame Retardant Polymer Nanocomposites. *Molecules* 26, 57. doi:10.3390/molecules26154670

Yu, B., Shi, Y., Yuan, B., Qiu, S., Xing, W., Hu, W., et al. (2015). Enhanced thermal and Flame Retardant Properties of Flame-Retardant-Wrapped Graphene/epoxy Resin Nanocomposites. *J. Mater. Chem. A.* 3, 8034–8044. doi:10.1039/c4ta06613h

Zhang, P., Hu, Y., Song, L., Ni, J., Xing, W., and Wang, J. (2010). Effect of Expanded Graphite on Properties of High-Density Polyethylene/paraffin Composite with Intumescent Flame Retardant as a Shape-Stabilized Phase Change Material. *Solar Energ. Mater. Solar Cells* 94, 360–365. doi:10.1016/j.solmat.2009.10.014

Zhang, S., Ding, F., Wang, Y., Ren, X., and Huang, T.-S. (2020). Antibacterial and Hydrophilic Modification of PET Fabrics by Electron Beam Irradiation Process. *Fibers Polym.* 21, 1023–1031. doi:10.1007/s12221-020-9765-3

Zhang, Y., Jing, J., Liu, T., Xi, L., Sai, T., Ran, S., et al. (2021). A Molecularly Engineered Bioderived Polyphosphate for Enhanced Flame Retardant, UV-Blocking and Mechanical Properties of Poly(lactic Acid). *Chem. Eng. J.* 411, 128493. doi:10.1016/j.cej.2021.128493

Conflict of Interest: The authors declare that the research was conducted in the absence of any commercial or financial relationships that could be construed as a potential conflict of interest.

Publisher's Note: All claims expressed in this article are solely those of the authors and do not necessarily represent those of their affiliated organizations, or those of the publisher, the editors and the reviewers. Any product that may be evaluated in this article, or claim that may be made by its manufacturer, is not guaranteed or endorsed by the publisher.